Conformational Stability of a Thrombin-Binding Peptide Derived from the Hirudin C-Terminus†

Feng Ni,* Daniel R. Ripoll, and Enrico O. Purisima

Protein Engineering Section, Biotechnology Research Institute, National Research Council of Canada, Montrēal, Quēbec, Canada H4P 2R2

Received June 21, 1991; Revised Manuscript Received November 25, 1991

ABSTRACT: The COOH-terminal region of hirudin represents an independent functional domain that binds to an anion-binding exosite of thrombin and inhibits the interaction of thrombin with fibrinogen and regulatory proteins in blood coagulation. The thrombin-bound structure of the peptide fragment, hirudin 55–65, has been determined by use of transferred NOE spectroscopy [Ni, F., Konishi, Y., & Scheraga, H. A. (1990) *Biochemistry 29*, 4479–4489]. The stability of the thrombin-bound conformation has been characterized further by a combined NMR and theoretical analysis of the conformational ensemble accessible by the hirudin peptide. Medium- and long-range NOE's were found for the free hirudin peptide in aqueous solution and in a mixture of dimethyl sulfoxide and water at both ambient (25 °C) and low (0 °C) temperatures, suggesting that ordered conformations are highly populated in solution. The global folding of these conformations is similar to that in the thrombin-bound state, as indicated by NOE's involving the side-chain protons of residues Phe(56), Ile(59), Pro(60), Tyr(63), and Leu(64). Residues Glu(61), Glu(62), Tyr(63), and Leu(64) all contain ~50% of helical conformations calculated from the ratio of the sequential d_{NN} and $d_{\alpha N}$ NOE's. Among the helical ensemble, active 3_{10}-helical conformations were found by an analysis of the medium-range [$(i,i+2)$ and $(i,i+3)$] NOE's involving the last six residues of the peptide. An analysis of the side-chain rotamers revealed that, upon binding to thrombin, there may be a rotation around the αCH–βCH bond of Ile(59) such that Ile(59) adopts a gauche$^-$ ($\chi_1 = +60$) conformation in contrast to the highly populated trans ($\chi_1 = -60$) found for Ile(59) in the free peptide. However, the thrombin-bound conformation of the hirudin peptide is still an intrinsically stable conformer, and the preferred conformational ensemble of the peptide contains a large population of the active conformation. The apparent preference for a gauche$^-$ ($\chi_1 = +60$) side-chain conformation of Ile(59) in the bound state may be explained by the existence of a positively charged arginine residue among the hydrophobic residues in the thrombin exosite.

Thrombin is the central regulatory enzyme in blood coagulation and haemostasis (Fenton, 1981). It is a trypsin-like serine protease, highly specific for the Arg–Gly peptide bonds cleaved during the conversion of the circulating fibrinogen to the fibrin clot (Scheraga, 1986). The specificity of thrombin toward fibrinogen is determined, in part, by the complicated surface topology around the active site of thrombin (Bode et al., 1989) and by the unique structural features of fibrinogen near the Arg–Gly peptide bonds (Ni et al., 1989a–c). Thrombin also interacts with fibrinogen (and fibrin) via a so-called anion-binding exosite which is distinct from the catalytic active site (Kaminski & McDonagh, 1983; Berliner et al., 1985; Kaminski & McDonagh, 1987; Fenton et al., 1988). This thrombin exosite has been implicated for the inflammatory effects of thrombin on endothelial cells (Prescott et al., 1990) and for the binding of thrombin to heparin cofactor II (Hortin et al., 1989), thrombomudulin (Tsiang et al., 1990; Hayashi et al., 1990), leuserpin-2 (Ragg et al., 1990), and platelet and endothelial cell receptors (Vu et al., 1991).

Hirudin is a very potent thrombin inhibitor of 65 amino acid residues found in the leech *Hirudo medicinalis* (Markwardt, 1970). Its high affinity for thrombin is a result of the concerted bivalent binding of the NH_2-terminal domain of hirudin to the thrombin active site and the COOH-terminal region of hirudin to the anion-binding exosite (Rydel et al., 1990; Grütter et al., 1990). Isolated fragments corresponding to the NH_2-terminal and the COOH-terminal domains of hirudin were found to bind to thrombin independently (Krstenansky et al., 1987; Mao et al., 1988; Maraganore et al., 1989; Chang et al., 1990a,b; Dodt et al., 1990; Dennis et al., 1990). The NH_2-terminal domain of hirudin offers promise for the design of thrombin-specific anticoagulants using protein engineering methodologies (Chang, 1990). Hirudin COOH-terminal peptides, on the other hand, can lead to inhibitors that are specifically targeted toward the thrombin exosite (Maraganore et al., 1989; Krstenansky et al., 1990) and that are invaluable for the study of the regulatory functions of thrombin (Hortin et al., 1989; Naski et al., 1990; Prescott et al., 1990; Jakubowski & Maraganore, 1990). Hirudin peptides can also be linked to small active site-directed inhibitors of thrombin to create molecules that bind to the active site and the exosite of thrombin simultaneously (Maraganore et al., 1990; DiMaio et al., 1990, 1991; Yue et al., 1991).

Recent structure–activity studies have emphasized the importance of ionic interactions in the binding of thrombin to hirudin. It was shown that hirudin binding prevents the chemical modification of the lysines in the exosite of thrombin (Chang, 1989). Mutagenesis studies revealed that negatively charged residues such as Glu in the COOH-terminal region of hirudin play a major role in determining the binding affinity, particularly in increasing the association rate constant with thrombin (Stone & Hofsteenge, 1986; Braun et al., 1988; Stone et al., 1989). The dissociation rate constant, on the other hand, is not much affected by the ionic strength of the solution or by the nature of the charged residues in the hirudin COOH

† NRCC Publication No. 33692.

* Author to whom correspondence should be addressed.

0006-2960/92/0431-2545$03.00/0

terminus (Stone & Hofsteegne, 1986; Braun et al., 1988). This result indicates that hydrophobic interactions may also be important in the stabilization of the thrombin–hirudin complex. Indeed, all of the hydrophobic residues were found to be important in determining the anticoagulant activities of exosite-binding hirudin peptides (Krstenansky et al., 1987, 1990; Ni et al., 1990). In the thrombin-bound state, hirudin COOH-terminal peptides fold into an amphiphilic structure with hydrophobic residues directly in contact with thrombin (Ni et al., 1990). These hydropobic contacts also constitute a major fraction of the interacting surface in the complex of thrombin with intact hirudin (Rydel et al., 1990).

In contrast to the thrombin-bound state, little information is available about the solution conformation of the hirudin COOH terminus in the uncomplexed state. The question still remains as to whether the bound conformation of the hirudin peptides is induced by binding to thrombin or is intrinsically stable in solution. We have characterized the conformational preferences of hirudin 55–65, both in aqueous solution and in mixed solvents. In this paper, we report the results of NMR experiments that led to the identification of the thrombin-recognized conformation in the free peptide. Furthermore, both molecular dynamics simulations and Monte Carlo searches were carried out to assess the stability of the active conformation of the hirudin peptide.

Experimental Procedures

Sample Preparation. The peptide fragment, (acetyl-Asp-Phe-Glu-Glu-Ile-Pro-Glu-Glu-Tyr-Leu-Gln-COOH or called hirudin 55–65) was synthesized and purified as described previously (Ni et al., 1990). Weighted amounts (1–10 mg) of the peptide were dissolved in 450 μL of an aqueous solution that was 150 mM in NaCl, 50 mM in sodium phosphate, and 0.2 mM in EDTA[1] at pH 5.3. A volume of 50 μL of the corresponding D_2O solution was added to provide the deuterium lock signal for the NMR spectrometer. The final pH's of the samples were checked and, if necessary, adjusted to 5.3 using trace amounts of dilute NaOH and HCl solutions. For samples in the mixed solvent, the peptide was first dissolved in 333 μL of fully deuterated DMSO. A volume of 167 μL of the aqueous solvent was then added to the DMSO solution so that the ratio of DMSO to H_2O (or D_2O) is 2:1, a condition with a large increase in solvent viscosity (Neuhaus & Williamson, 1989).

NMR Data Acquisition and Processing. All two-dimensional NMR experiments were carried out using procedures described in our previous paper (Ni et al., 1990). To increase the sensitivity of ROESY experiments, the spectrometer was configured in the inverse mode with both the excitation and spin-lock pulses delivered from a three-level and fast-switching decoupler (Brüker). Spin-lock was achieved by a low-power (~2 kHz) continuous-wave rf pulse with carrier positioned at 4.8 ppm, which is far off from the center in between NH (~8.2 ppm)–αCH (~4.3 ppm) or αCH (~4.3 ppm)–βCH (~2.0 ppm) protons (Ni et al., 1990) so that no Hartmann–Hahn matching (HOHAHA effects) occurs between coupled spins (Bax & Davis, 1985; Neuhaus & Keeler, 1986). Off-resonance effects associated with low-power spin-locking were compensated by the insertion of 90°-hard pulses both before and after the spin-lock period (Criesinger & Ernst, 1987).

All FID matrices were acquired in sine-modulation along the t_1 direction (Otting et al., 1986). The initial t_1 delays were carefully adjusted so that phase corrections in the F_1 spectral dimension were exactly 90° and only 0th order (Marion & Bax, 1989). Residual solvent signals were further suppressed by use of a subtraction procedure (Marion et al., 1989) incorporating maximum entropy extrapolation (Ni & Scheraga, 1986) to improve the performance. The FID matrices were Fourier transformed and phase-corrected *first* along the t_1 dimension. The first five data points of each t_2 interferogram were then corrected using a maximum entropy (backward) extrapolation procedure (Ni & Scheraga, 1986) before Fourier transformation and phase correction. This treatment significantly reduced baseplane distortions caused by the transient response of the rf receiver (Marion & Bax, 1989). If necessary, F_2 spectral baselines were further corrected using a procedure reported recently (Dietrich et al., 1991). The ROESY FID matrices were multiplied by cosine square windows along both the t_1 and t_2 directions. These window functions were also used for the NOESY spectra of the peptide in H_2O and D_2O solutions at both 25 and 0 °C and for the spectra in DMSO/H_2O or DMSO/D_2O at 25 °C. Other spectra were processed by use of a 22.5°-shifted sine bell in the t_1 direction and a 45°-shifted sine bell in the t_2 direction.

Buildup rates for NOE's between well-resolved proton pairs were determined using the transient NOE technique, with modifications to compensate for spin diffusion and incomplete magnetization recovery (Andersen et al., 1987; Eaton & Andersen, 1987). The experiments were carried out employing NOE mixing times up to 500 ms. Cross relaxation rates were estimated from the linear region (up to a mixing time of 300 ms) of the plot of the residual driver normalized fractional enhancements versus the corresponding mixing times (Eaton & Andersen, 1987). Cross relaxation rates can also be estimated from the rate of the integrated intensities of NOE cross peaks and the corresponding diagonal peaks. Two methods were used for the calculation of the integrated intensities of two-dimensional peaks. One is the projection method reported in our previous work (Ni et al., 1989b,c). The second one involves an appropriate choice of an oval footprint around each peak within the 2d integration module of the FTNMR program (Hare Research, Inc.). This latter method was also adopted for the integration of well-resolved sequential $d_{\alpha N}$ and d_{NN} NOE's.

Proton Resonance Assignments, Temperature Dependence of NH Chemical Shifts, and $^3J_{HN\alpha H}$ and $^3J_{H\alpha\beta H}$ Coupling Constants. Sequence-specific assignments (Tables SI and SII in the Supplementary Material) of the proton resonances were established by an analysis of the cross-peak patterns in the NOESY (or ROESY) spectra of the free peptide. The NH chemical shifts of the hirudin peptide in both the aqueous and the mixed solvents decrease linearly with temperature within the range of 5–40 °C. The NH temperature coefficients (Table I) were determined by a regression analysis of the dependence of the NH chemical shift on temperature. The vicinal coupling constants, $^3J_{HN\alpha H}$, were determined from the fine structure of the NH–αCH cross peaks in COSY spectra using a newly developed method to minimize the effect of spectral line broadening (Kim & Prestegard, 1989). The COSY FID matrices were acquired with sizes of $400(t_1) \times 1024 \times 2(t_2)$ or $400(t_1) \times 2048 \times 2(t_2)$ in double-quantum

[1] Abbreviations: NMR, nuclear magnetic resonance; COSY, *J*-correlation spectroscopy; NOE, nuclear Overhauser effects; NOESY, two-dimensional nuclear Overhauser and exchange spectroscopy; ROESY, two-dimensional rotating-frame NOE spectroscopy; FID, free induction decay; HOHAHA, homonuclear Hartmann and Hahn magnetization transfer; DMSO, dimethyl sulfoxide; EDTA, ethylenediaminetetraacetic acid; MD, molecular dynamics; EDMC, electrostatically driven Monte Carlo; ECEPP, empirical conformational energy for polypeptides and proteins.

Table I: Coupling Constants,[a] $^3J_{HN\alpha H}$ and $^3J_{H\alpha\beta H}$, and Temperature Coefficients[b] of the Hirudin Peptide in Solution

	55 D	56 F	57 E	58 E	59 I	60 P	61 E	62 E	63 Y	64 L	65 Q
					(A) H_2O						
$^3J_{HN\alpha H}$	6.9	6.8	6.9	6.6	7.7		5.7	6.4	7.4	7.3	7.4
$^3J_{H\alpha\beta H}$											
(i)	8.8	8.5	8.9	8.7		8.2	8.6	8.1	8.7	10.0	8.4
(ii)	5.3	6.0	5.6	5.9	9.0	6.6	5.8	5.9	6.0	5.0	4.7
$\Delta\delta/\Delta T$	8.5	8.7	6.0	8.4	11.5		8.7	7.2	9.4	8.9	8.3
					(B) DMSO/H_2O						
$^3J_{HN\alpha H}$	7.7	7.6	7.5	7.9	7.3		6.3	7.0	8.2	8.1	7.8
$^3J_{H\alpha\beta H}$											
(i)	7.7	9.1	8.9	7.6[c]			8.5	9.6[c]	9.5	9.7[c]	9.0
(ii)	6.0	4.6	5.4	5.3[c]	9.4[c]		5.9	4.9[c]	4.5	4.9[c]	4.3
$\Delta\delta/\Delta T$	6.7	6.0	5.4	6.1	6.9		7.0	5.8	4.6	4.9	6.5

[a] The values of the coupling constants are in Hertz. The larger $^3J_{H\alpha\beta H}$ coupling constants (i) were assigned to the *pro-R* βCH protons for residues Phe(56), Tyr(63), and Leu(64), and the smaller ones (ii) to the *pro-S* βCH protons. Ile(59), on the other hand, has a large $^3J_{H\alpha\beta H}$ coupling constant for the single *pro-S* βCH proton. [b] Temperature coefficients are listed as $-10^3\Delta\delta/\Delta T$ (ppm/K). [c] These values were determined from a phase-sensitive β-COSY spectrum.

filtered and phase-sensitive modes. Before Fourier transformation, the data matrix was multiplied by a 90° phase-shifted sine bell along t_2 and by a 22.5° phase-shifted sine bell along t_1 and then extended with zeroes such that the digital resolution of the spectra was increased to 0.37 Hz/pt along both the F_1 and the F_2 spectral dimensions. Peak–peak separation was determined from a contour display of the cross peaks. This allowed interpolation between adjacent spectral slices to increase the precision of the $^3J_{HN\alpha H}$ values to ±0.2 Hz. The vicinal coupling constants, $^3J_{H\alpha\beta H}$, were determined from the peak–peak separation of well-resolved αCH and βCH multiplets in one-dimensional spectra of the peptide in deuterated solvents with a digital resolution of 0.15 Hz/pt. In the case of moderately overlapped peaks, the spectral resolution was enhanced by Lorentzian–Gaussian apodization or with a 3–4-Hz line width reduction achieved using a constrained deconvolution technique (Ni & Scheraga, 1989). Severely overlapped peaks were resolved by an analysis of the reduced multiplets in a phase-sensitive COSY spectrum with a small flip angle (β-COSY). The large dispersive diagonal associated with such a COSY spectrum was suppressed using time-domain convolution (Marion et al., 1989) of the t_1 interferograms with the diagonal peaks shifted to zero frequency.

Molecular Dynamics Simulations. Molecular dynamics simulations were carried out using the AMBER potential (Weiner et al., 1984) as implemented in SYBYL 5.32 (Tripos Associates, Inc.). A conformation of acetylhirudin 56–65-$NHCH_3$ satisfying distance constraints derived from transferred NOE experiments (Ni et al., 1990) was immersed in a 32.54-Å cubic box of preequilibrated TIP3P water molecules (Jorgensen et al., 1983). All calculations were carried out with periodic boundary conditions and a nonbonded cutoff of 8 Å. Ionizable groups were taken to be charged, and a dielectric constant $\epsilon = 1$ was used. Prior to the dynamics simulation, the system was energy-minimized to relieve bad intermolecular contacts. A constant volume and temperature dynamics simulation was then carried out using the Verlet algorithm (Verlet, 1967) with a time step of 2.0 fs and with all bond lengths constrained using SHAKE (Ryckaert et al., 1977). A thermalization period of 6.0 ps was used to bring the temperature of the system to 300 K. The system was then allowed to evolve for another 44 ps. All calculations were carried out on a Silicon Graphics 4D/280 computer.

Monte-Carlo Conformational Search. Searches of the low-energy conformations of the peptide acetylhirudin 56–65-$NHCH_3$ were carried out by use of the electrostatically driven Monte Carlo (EDMC) method (Ripoll & Scheraga, 1988, 1989). The geometry of the amino acid residues was assumed to be rigid with bond lengths and bond angles of the peptide chain fixed at their equilibrium values. Ionizable groups were considered to be neutral, but partial ECEPP/2 charges were assigned to every atom in the molecule. All the runs were carried out by considering the complete set of the backbone and the side-chain dihedral angles as independent variables. The potential energies and the geometry were computed with the ECEPP/2 algorithm (Momany et al., 1975; Némethy et al., 1983; Sippl et al., 1984). Energy minimizations were carried out with the algorithm SUMSL (Secant Unconstrained Minimization Solver) (Gay, 1983).

Results

NOE's of Hirudin 55–65 in Aqueous Solution. In the previous study, very few NOE's were observed for the peptide fragment hirudin 55–65 free in solution (Ni et al., 1990). To optimize experimental conditions, one-dimensional transient NOE's were measured for proton pairs on the peptide backbone, particularly for those with a fixed interproton distances such as the Pro δCH_2 protons which have a separation of 1.78 Å as determined by the covalent geometry (Momany et al., 1975). From the NOE buildup curve, the cross relaxation rate between these protons was estimated to be 0.55 s^{-1} for the peptide in aqueous solution at 25 °C. This relaxation rate corresponds to a rotational correlation time (τ_c) of 0.56 ± 0.05 ns for the proton pair, in good agreement with a predicted correlation time of 0.6 ns for the peptide in the monomeric state with a molecular mass of 1457 daltons (Cantor & Schimmel, 1980). Thus, the hirudin peptide is very near the null region (τ_c = 0.36 ns) of normal NOESY experiments, resulting in the absence of many NOE's in the NOESY spectra of the free peptide in aqueous solution (Bothner-By et al., 1984).

NOE's between protons nearby in space can be observed by use of the rotating-frame NOE experiment (ROESY) that is less sensitive to the tumbling rate (Bothner-By et al., 1984). ROESY spectra were thus obtained for the peptide in both H_2O and D_2O solutions at 25 °C. All the cross peaks had opposite signs compared to the diagonal peaks in all spectra with spin-lock periods (τ_m) from 100 to 400 ms (Figure 1). This indicated the absence of spin-diffusion cross peaks which would appear in ROESY spectra with the same sign as the diagonal peaks (Bax et al., 1986; Farmer et al., 1987). With a short mixing time (τ_m < 120 ms), all the cross peaks are due to sequential and intraresidue NOE's between both coupled and uncoupled protons and appear on the opposite side of the

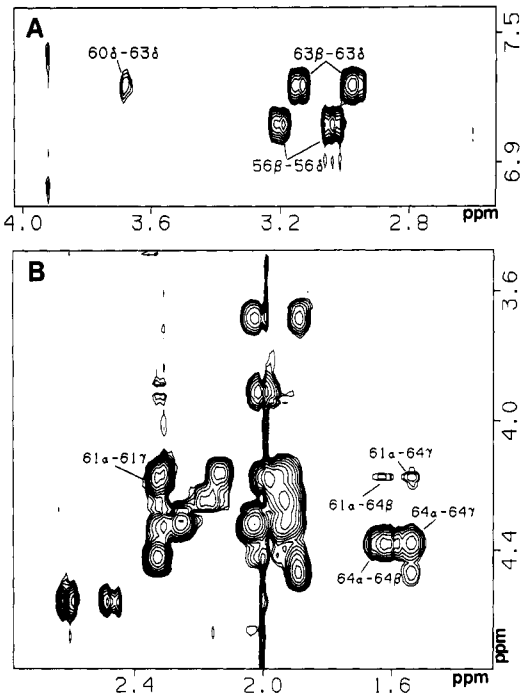

FIGURE 1: Selected NOE's between the side-chain protons of hirudin 55–65 in aqueous (D_2O) solution at 25 °C and pD 5.2. The concentration of the peptide was 6 mM, and the spectrum was acquired using the rotating-frame NOE (ROESY) technique. The medium- and long-range NOE's are indicated by the residues involved. The label 60δ–63δ, for example, refers to the NOE between one of the δCH_2 protons of Pro(60) and the δCH_2 ring protons of Tyr(63). All the cross peaks are negative relative to those of the diagonal peaks which were phased to have positive intensities. The cross peaks identified as medium-range NOE's are also present in the symmetry-related locations of the two-dimensional ROESY spectra (not shown). (A) The ROESY spectrum was acquired with a spin-lock period of 200 ms. (B) The spin-lock time employed was 400 ms. Similar NOE's are also present in the ROESY spectra of the peptide in H_2O solution at pH 4.5 with mixing times between 200 and 400 ms (not shown).

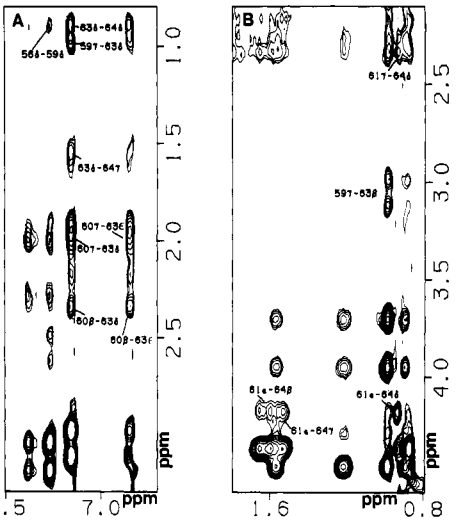

FIGURE 2: Medium- and long-range NOE's of hirudin 55–65 at 0 °C. The peptide sample was the same as indicated in Figure 1 and the NOE spectrum was acquired by use of the standard NOESY technique with a mixing time of 500 ms. These NOE's are also present in the NOESY spectra of the peptide in H_2O solution at pH 4.5. (A) Cross peaks between aromatic protons and the side-chain aliphatic (β, γ, δ) protons. (B) Cross peaks between αCH and side-chain protons.

diagonal (spectra not shown). Thus, direct HOHAHA effects were avoided by the use of a weak spin-lock pulse and by the positioning of the rf carrier frequency away from the center of coupled protons (Bax & Davis, 1985). At longer mixing times ($\tau_m \geq 200$ ms), medium-range NOE's become observable which include NOE contacts between the δCH_2 protons of Pro(60) and the δCH_2 protons of Tyr(63) (Figure 1A), between the αCH proton of Glu(61) and the βCH_2 protons of Leu(64), and between the αCH proton of Glu(61) and the γCH proton of Leu(64) (Figure 1B). With $\tau_m = 400$ ms, there are also *reproducible* weak medium-range backbone NOE's between the αCH proton of Pro(60) and the NH proton of Glu(62), between the αCH proton of Glu(62) and the NH proton of Leu(64), between the αCH proton of Tyr(63) and the NH proton of Gln(65), and between the αCH proton of Glu(61) and the NH proton of Leu(64) (spectra not shown). Other weak NOE's include those between the δCH_2 protons of Phe(56) and the δCH_3 protons of Ile(59) and between the δCH_3 and γCH_3 protons of Ile(59) and the δCH_2 protons of Tyr(63). These weak NOE's were interpreted only when similar NOE's were observed for the peptide under different experimental conditions (see the following sections).

NOE experiments were subsequently carried out at low temperature, where molecular tumbling of the peptide is sufficiently slow ($\tau_c \sim 0.8$ ns at 0 °C) so that sizable NOE's can be observed with the normal NOESY technique. As in the ROESY experiment, there are indeed medium- and long-range NOE's between the side-chain protons of residues Phe(56), Ile(59), Pro(60), Glu(61), Tyr(63), and Leu(64) for the free peptide at 0 °C (Figure 2). These NOE's appear to be selective and could not be due to spin diffusion since, for example, there are no cross peaks between the γCH_2 protons of Ile(59) and the δCH_2 and ϵCH_2 protons of Tyr(63) even though other NOE's are present between side-chain protons of these two residues (Figure 2A). Other NOE's include the interactions between the γCH_3 protons of Ile(59) and the βCH_2 protons of Tyr(63) and those between the αCH proton of Glu(61) and the βCH_2, γCH, and δCH_3 protons of Leu(64) (Figure 2B). There are also medium-range NOE's (spectra not shown) between the αCH and NH protons [$d_{\alpha N}(i,i+2)$] of residues Pro(60) and Glu(62), Glu(61) and Tyr(63), Glu(62) and Leu(64), and Tyr(63) and Gln(65); NOE's between the NH protons [$d_{NN}(i,i+2)$] of residues Glu(61) and Tyr(63), and Glu(62) and Leu(64); and NOE's [$d_{\alpha N}(i,i+3)$] between the αCH proton of Glu(61) and the NH proton of Leu(64). These NOE's are unique to the hirudin peptide under study since they are absent in the NOESY spectra of an analogue of the hirudin peptide where the essential residue Ile(59) is replaced by a Gly residue (Ni, Szewczuk, and Konishi, manuscript in preparation).

NOE's of Hirudin 55–65 in DMSO/H_2O. For the free peptide in aqueous solution, some NOE's are still very weak even at a low temperature of 0 °C. This can be seen in Figure 2B for the NOE cross peaks between the αCH proton of Glu(61) and the side-chain protons of Leu(64). These NOE's may become more easily observable if the tumbling rate of the peptide can be further decreased by adding a cosolvent such as DMSO under the condition that the organic solvent does not change the structure of the peptide (Neuhaus & Williamson, 1989). As seen in Figure 3, there are still characteristic NOE's between the side-chain protons of residues Phe(56), Ile(59), Pro(60), Tyr(63), and Leu(64) for the hirudin peptide in a 2:1 mixture of DMSO with the aqueous solvent (H_2O or D_2O) at both 25 °C ($\tau_c \sim 1.4$ ns) and 0 °C ($\tau_c \sim 6$ ns) even with a shorter mixing time of 200 ms. The NOE's between residues Glu(61) and Leu(64) were indeed stronger (spectra not shown) than those observed in aqueous

Table II: Backbone NOE's Observed for the Hirudin Peptide in the Thrombin-Bound State and in Solution[a]

hirudin 55–65	55 D	56 F	57 E	58 E	59 I	60 P	61 E	62 E	63 Y	64 L	65 Q
d_{NN}	?/?	m/?	m/m	−/?	−/w	−/w	m/m	m/m	m/m	m/m	
$d_{NN}(i,i+2)$	?/−	?/?	?/?	−/−	−/−	?/−	?/w	w/w	w/w		
$d_{\alpha N}(i,i+2)$	?/−	?/?	?/−	−/−	−/?	w/w	w/w	w/w	w/w		
$d_{\alpha N}(i,i+3)$	−/−	−/−	−/−	−/−	−/−	−/?	w/w	−/−			
$d_{\alpha\beta}(i,i+3)$	−/−	−/−	−/−	−/−	−/−	−/−	m/w	m/?			

[a] w, weak intensities; m, medium intensities; −, nonexistent; ?, not resolved. For NOE's involving the proline residue, the δCH_2 protons are used in place of the NH protons of other residues. The labels to the left of the slashes pertain to the NOE's of the peptide in the thrombin-bound state, identified here by an enhanced processing of the transferred NOESY spectrum acquired in the previous study (Ni et al., 1990). The labels to the right of the slashes correspond to the NOE's of the free peptide in both the aqueous and the mixed solvents.

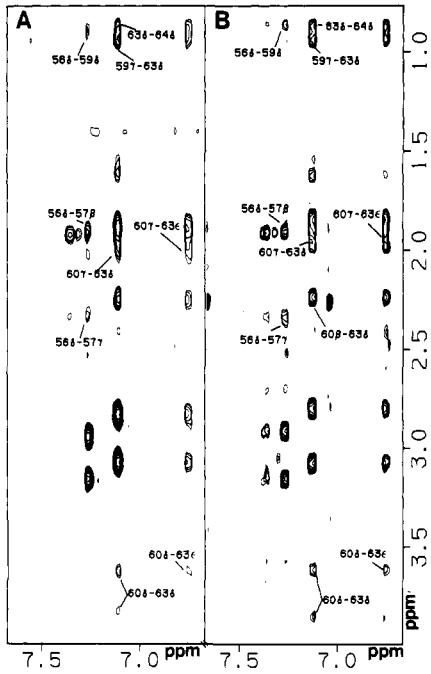

FIGURE 3: NOE map between the aromatic and the side-chain aliphatic protons of hirudin 55–65 in a 2:1 mixture of DMSO and the aqueous (H_2O) solvent. The medium- and long-range NOE's are indicated by the residues involved. (A) The NOESY spectrum was acquired at 25 °C with a mixing time of 500 ms. But shorter mixing times (200 and 300 ms) were also used to assess the effects of spin diffusion. (B) The NOESY spectrum was acquired at 0 °C with a shorter mixing time of 200 ms. Similar NOE's are also present in all the NOESY spectra of the peptide in the DMSO/D_2O solvent with mixing times between 200 and 500 ms.

solution (Figure 2B). The increase in NOE intensities makes other NOE's more easily identified. These include, for example, NOE's between the side-chain protons of residues Phe(56) and Glu(57) and those between the δCH_2 protons of Pro(60) and the ϵCH_2 protons of Tyr(63) (Figure 3B). The NOE's observed in the mixed solvent are again selective since a single amino acid substitution from Ile(59) to Gly(59) results in the disappearance of many of the NOE cross peaks (Ni, Szewczuk, and Konishi, manuscript in preparation). Furthermore, these nonsequential NOE's and others identified in both the aqueous and the mixed solvents are identical, and *both* are very similar to those observed for the peptide in the thrombin-bound state (Table II).

Conformations of Hirudin 55–65 in Solution. A short linear peptide such as hirudin 55–65 usually does not adopt a unique structure in solution. No extreme values were observed for the $^3J_{HN\alpha H}$ and $^3J_{H\alpha\beta H}$ coupling constants (Table I), a result indicating that conformational averaging is taking place for the peptide in solution (Bystrov, 1976). Only residue Glu(61) has a smaller coupling constant of 5.7 Hz in water, a value weighted toward that (3.9 Hz) observed for a turn conformation at residues Pro(60) and Glu(61) (Wagner et al., 1984). The temperature coefficient of the NH proton of Glu(62) is slightly reduced compared to other nearby residues, indicating that this proton may be shielded from the solvent by a local structure at residues Pro(60), Glu(61), and Glu(62) in a significant population of the free peptide. In the mixed solvent, there is a uniform decrease in the NH temperature coefficients, a phenomenon that may be a result of the decrease in the rate of proton exchange due to the increased hydrogen bonding between the H_2O and DMSO solvent molecules.

The observation of medium- and long-range NOE's (Figures 1–3; Table II) indicates that the hirudin peptide can fold into a compact structure in a significant population within the conformational ensemble of the free peptide. The nonpolar side chains of residues Phe(56), Ile(59), Pro(60), Tyr(63), and Leu(64) form a continuous hydrophobic cluster, as indicated by the NOE's between the side-chain protons of these residues (Figures 1–3). Furthermore, residues Glu(61)–Gln(65) may fold into 3_{10}-helical conformations as suggested by the $(i,i+2)$ NOE's identified here for the peptide in both free and the thrombin-bound states (Table II). This helical structure is apparently very stable since all of the characteristic medium- and long-range NOE's exist both in the aqueous solution and in the mixed solvent. Recently, it was shown that the helical content of a peptide may be estimated from the ratio of the integrated intensities of the sequential NOE's, $d_{\alpha N}$ and d_{NN} involving each residue (Bradley et al., 1990). Using this method, residues Glu(61), Glu(62), Tyr(63), and Leu(64) were found to be in helical states in about 50% of the conformational ensemble of the hirudin peptide in both the aqueous and the mixed solvents. This is in a seeming contradiction to the previous observation that there is no significant helical content in the CD spectra of the hirudin peptides (Mao et al., 1988; Krstenansky et al., 1988). Peptide–peptide aggregation may lead to structure formation of the free peptide at the concentration range of 5–10 mM used in NOE measurements. This is unlikely since the NH proton resonances of the peptide remain sharp and well-resolved for samples with 0.5 mM up to 10 mM in peptide concentration (spectra not shown). From measurement of cross relaxation rates (see the previous section), it was found that the peptide in aqueous solution tumbles with a rotational correlation time of ~0.6 ns, indicating that it is monomeric at a concentration up to 10 mM. A more reasonable explanation of the discrepancy in helical contents deduced from CD and NMR measurements is that the folded conformation of hirudin 55–65 contains turns and extended regions whose CD spectra may obscure the detection of helices (Bradley et al., 1990). Moreover, the presence of a tyrosine residue in hirudin 55–65 may also significantly decrease the helical content in the CD spectra.

On the basis of the measurement of transferred NOE's, we have determined the thrombin-bound conformation of residues 56–65 of the hirudin COOH terminus (Ni et al., 1990). The

global folding of the bound peptide is well-defined with a nonpolar surface organized by the side chains of residues Phe(56), Ile(59), Pro(60), Tyr(63), and Leu(64). Distance-geometry calculations showed that the side chains of residues Ile(59), Tyr(63), and Leu(64) are all fixed around a single orientation: $\chi_1 = +60$ for Ile(59) (gauche$^-$ with respect to the γCH_3 group) and $\chi_1 = -60$ for both Tyr(63) and Leu(64) (gauche$^-$ with respect to the γCH group). The side chain of Phe(56) is not as defined, but it has a tendency to adopt the gauche$^-$ χ_1 state as observed in the crystal structure of the thrombin–hirudin complex (Rydel et al., 1990). In solution, the side chains of all the residues appear to average among the three staggered χ_1 rotameric states, as indicated by the measured values of the $^3J_{H\alpha\beta H}$ coupling constants (Table I). Assuming that the upfield and downfield resonances for Tyr(63) correspond to the *pro-R* and *pro-S* βCH protons, respectively, the *pro-R* protons would have the larger $^3J_{H\alpha\beta H}$ coupling constants for the peptide in aqueous solution. On the basis of these prochiral assignments, the relative populations (Pachler, 1963) of the three χ_1 rotameric states for Tyr(63) were estimated to be 54% for $\chi_1 = -60$ (gauche$^-$), 30% for $\chi_1 = \pm 180$ (trans) and 16% for $\chi_1 = +60$ (gauche$^+$). Similarly for Leu(64), the corresponding values are 65% (gauche$^-$), 21% (trans), and 14% (gauche$^+$). With Phe(56), these populations are 52% (gauche$^-$), 30% (trans), and 18% (gauche$^+$). The higher contents for the gauche$^-$ state are in good agreement with those determined previously for hydrophobic residues in small peptides (Fischman et al., 1978; Cowburn et al., 1983; Stimson et al., 1986). For Ile(59), the single *pro-S* βCH proton has a rather large coupling constant to the αCH proton in contrast to those observed for Tyr(63) or Leu(64) (Table I). The population of the $\chi_1 = -60$ (trans with respect to the γCH_3 group) is estimated to be 60% with a total of 40% for the unresolved gauche$^-$ and gauche$^+$ states. Thus, with Phe(56), Tyr(63), and Leu(64), the side-chain conformations selected by thrombin binding are also the preferred ones for the free peptide in solution. With Ile(59), however, the bound state (gauche$^-$) is apparently the lower populated one (<40%) in solution.

The side-chain conformation of Ile(59) was further examined using NOE data in both the free and the thrombin-bound states. In solution, there are NOE's of medium intensities between the γCH_3 protons of Ile(59) and the βCH_2 protons of Tyr(63) (Figures 2B and 4A). These NOE's become very weak for the peptide in the thrombin-bound state compared to the NOE's between the βCH_2 protons of Tyr(63) and the δCH_3 of Ile(59) and/or one set of the two δCH_3 protons of Leu(64) (Figure 4B). For the free peptide, there also exist NOE's between the γCH_3 protons of Ile(59) and the NH protons of residues Glu(61) and Glu(62) (Figure 4A). Upon binding to thrombin, these NOE's involving Ile(59) are replaced by a weak NOE between the δCH_3 protons of Leu(64) and the NH protons of Glu(61) and/or Glu(62) (Figure 4B). Furthermore, the sequential NOE's between the γCH_3 protons of Ile(59) and the δCH_2 protons of Pro(60) become weaker for the peptide upon binding to thrombin. These NOE differences suggest that there is indeed a conformational change of the side chain of Ile(59) upon binding to thrombin, in agreement with the analysis based on the $^3J_{H\alpha\beta H}$ coupling constant of Ile(59).

Dynamic Stability of Hirudin 56–65: Molecular Dynamics and Monte Carlo Simulations. To further investigate the stability of the bound conformation for the free peptide in solution, we carried out a molecular dynamics simulation of the solvated peptide starting from a conformation satisfying

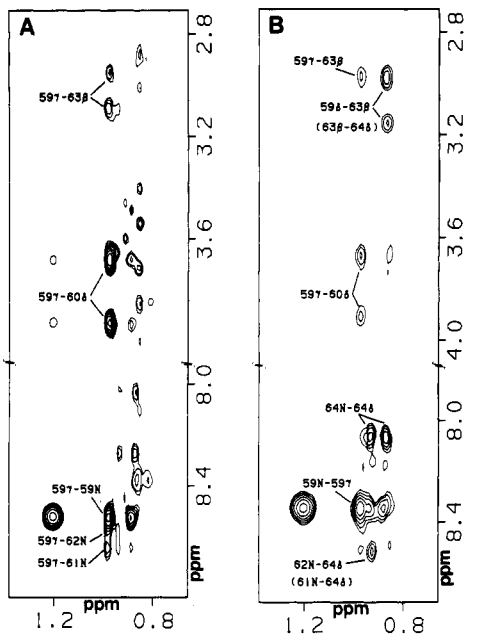

FIGURE 4: Comparison between the NOE's involving the side-chain protons of Ile(59) for the free peptide and for the peptide in the presence of thrombin. (A) NOE's of the free peptide in the aqueous (H_2O) solution at 0 °C. The experimental conditions were similar to those noted in the legend to Figure 2. These NOE's were also observed for the peptide in the DMSO/H_2O solvent (spectra not shown). (B) Corresponding transferred NOE's in the presence of thrombin. The spectrum was obtained with the NOESY technique at 25 °C with a mixing time of 200 ms. Detailed experimental conditions were described previously (Ni et al., 1990).

distance constraints derived from transferred NOE experiments (Ni et al., 1990). This starting conformation has an amphiphilic character with a nonpolar surface formed by the side chains of residues Phe(56), Ile(59), Pro(60), Tyr(63), and Leu(64). Without any distance constraints, the hydrophobic cluster and the helical region of the peptide remained intact throughout the course (up to 52.6 ps) of the molecular dynamics simulation (Figure 5). Residues Phe(56), Glu(57), and Glu(58), on the other hand, showed large variability in their positions relative to the seven well-defined residues, Ile(59)–Gln(65). The helical region of the peptide fluctuated between a 3_{10}- and an α-helix with the backbone carbonyl of Pro(60) alternating between (i,i+3) and (i,i+4) hydrogen bonds with the Tyr(63) and Leu(64) amide hydrogens, respectively. However, the side chain of Ile(59) remained at the gauche$^-$ ($\chi_1 = +60$) conformation throughout the simulation (Figure 5).

A search of the conformational space of the peptide was also carried out using the electrostatically driven Monte Carlo (EDMC) method (Ripoll & Scheraga, 1988, 1989). This method provides a collection of low-energy local minima which can be analyzed to provide a qualitative characterization of accessible conformations of the hirudin peptide. The calculation was carried out without distance constraints but utilized, as the starting conformation, an energy-minimized structure of hirudin 56–65 generated by restrained energy minimization incorporating the transferred NOE distance constraints determined previously (Ni et al., 1990). The converged conformations consistently contained the 3_{10}-helical backbone structures at residues Glu(61)–Gln(65). Ile(59) also retained the gauche$^-$ side-chain conformation as in the starting state.

Conformational searches were also carried out using a restrained EDMC methodology (Ripoll & Ni, 1992) incorporating the NOE's of the free peptide (Figures 1–3, Table II) as weak distance constraints. These calculations led to con-

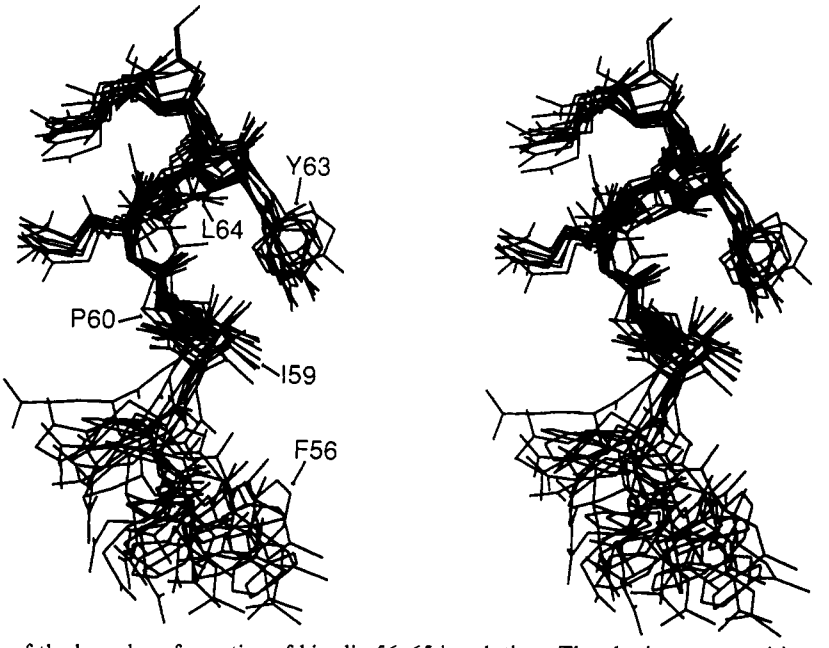

FIGURE 5: Dynamic stability of the bound conformation of hirudin 56–65 in solution. The plot is a superposition of 11 conformations taken every 4 ps between 10 and 50 ps along the molecular dynamics trajectory of hirudin 56–65 in water. To emphasize structural fluctuations of residues Phe(56)–Glu(58), the superposition was carried out using only the C^{α} atoms of residues Ile(59)–Gln(65).

formations of low energies (−86 kcal/mol) with a well-defined 3_{10}-helical segment at residues Glu(61)–Gln(65). In all these conformations, Ile(59) consistently assumes an approximately trans ($\chi_1 = -60$) side-chain conformation in contrast to that determined on the basis of transferred NOE's. To assess structural features of other low-energy conformations, EDMC calculations were carried out starting from randomly generated conformations of the peptide. These searches converged to conformations of comparable or lower energies (−86 to −94 kcal/mol) relative to that of the constrained conformation. These conformations all contained a trans ($\chi_1 = -60$) Ile(59) in contrast to residues Tyr(63) and Leu(64) with which both the gauche$^-$ and the trans side-chain conformations were observed with high frequency (unpublished observations). Furthermore, α-helical conformations were observed during some of the runs, indicating both α- and 3_{10}-helical backbone conformations are energetically accessible for residues Glu(61)–Gln(65). Other low-energy conformations, however, do not contain a helical segment within residues Glu(61)–Gln(65), in agreement with the partial helicities for these residues determined experimentally (see the previous section). Thus, both experimental and theoretical results support the assumption that the hirudin peptide can adopt an ensemble of low-energy conformations. This ensemble of conformations contains the one that is recognized by thrombin.

Discussion

The solution structures of both the native and recombinant hirudins have been determined by use of two-dimensional NMR spectroscopy in an attempt to understand the specific binding between thrombin and hirudin (Clore et al., 1987; Haruyama & Wüthrich, 1989; Folkers et al., 1989). Only the disulfide-linked core of residues 3–30 and residues 37–48 was found to assume a well-defined structure. Few NMR constraints were detected concerning the solution conformation of residues 49–65 in the hirudin COOH terminus. In the complex, residues Asp(55)–Gln(65) adopt well-defined structures as shown by transferred NOE's of the peptide from the complex (Ni et al., 1990). The thrombin-bound conformation of the hirudin COOH-terminal residues determined by transferred NOE's are very similar to those observed in the crystal of the complex of thrombin with intact hirudin (Rydel et al., 1990). In the current study, stable and orderred conformations were found for the free hirudin peptide in both aqueous solution and in a mixed solvent. These observations are in contradiction to the previous conclusion that the hirudin COOH terminus is primarily disordered in solution (Clore et al., 1987; Haruyama & Wüthrich, 1989; Folkers et al., 1989). The absence of these conformations in intact hirudins could be a result of transient interactions between the core and the COOH terminus of hirudin as observed previously (Haruyama et al., 1989). An alternative explanation may be that the local motions of residues 49–65 are such that the COOH-terminal region, residues 55–65, behaves like a small peptide attached to the hirudin core through the hinge residues 49–54. Fast tumbling of the hirudin C-terminal tail would preclude the observation of NOE's with the standard NOESY technique used in the previous studies (Sukumaran et al., 1987; Haruyama & Wüthrich, 1989; Folkers et al., 1989). Indeed, few NOE's were observed involving residues Asn(52), Asp(53), and Gly(54) even in the thrombin-bound state, suggesting that these residues move freely in the complex (Ni et al., 1990), in agreement with the X-ray observation that these residues have very poor electron density in the crystal of the complex between human thrombin and the intact hirudin (Rydel et al., 1990).

There is now ample experimental evidence that short linear peptides and protein fragments can assume organized local structures in aqueous solution (Wright et al., 1988). These local structures include hydrophobic clusters, short turns, and helical structures. To understand the forces that stabilize peptide conformation, it is very important to find out the relationship between ordered structures of free peptides and those they adopt when these peptides are part of (or when they bind to) a protein. Attempts have been made to correlate the free and bound conformations of peptide ligands using both NMR and X-ray crystallographic methods. In some of the systems, there seem to be significant conformational changes in the ligands upon binding to the respective protein acceptors (Dyson et al., 1988; Stanfield et al., 1990). In the current study, it is demonstrated that the *linear* hirudin peptide can also adopt a highly populated conformation in solution with

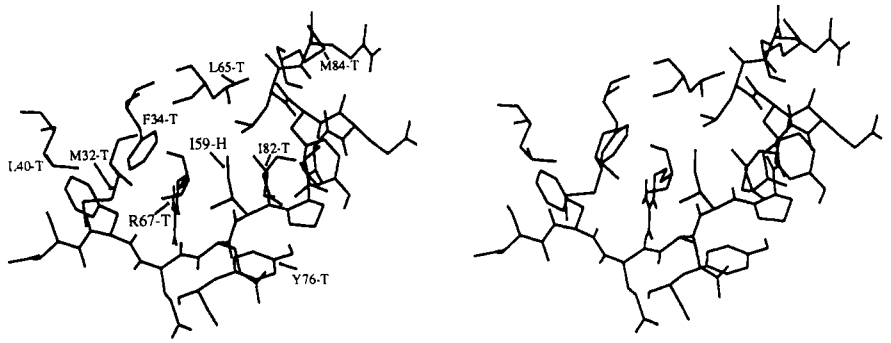

FIGURE 6: Interaction of hirudin 55–65 with the thrombin exosite. The modeling of the complex was described elsewhere (Yue et al., 1991). All thrombin residues are identified with "-T" and I59-H refers to residue Ile(59) of the hirudin peptide.

structural features that are very similar to those recognized by thrombin. In the thrombin-bound state, the hirudin COOH terminus folds into an amphiphilic conformation with significant nonpolar contacts with the thrombin exosite (Figure 6). This bound conformation may be stabilized by hydrophobic interactions with the thrombin residues Met(32), Phe(34), Leu(40), Leu(65), Tyr(76), Ile(82), and Met(84) (Bode et al., 1989; Rydel et al., 1990). However, the nonpolar side chains of the hirudin peptide are also organized to form a hydrophobic cluster in solution in the absence of thrombin, as suggested by NOE's between the side-chain protons of residues Phe(56), Ile(59), Pro(60), Tyr(63), and Leu(64) (Figures 1–3). Furthermore, the backbone conformations of residues Pro(60)–Gln(65) remain intact in the free peptide, as indicated by extensive NOE's involving these residues (Table II). These structural features are intrinsically stable during molecular dynamics simulations (Figure 5) and are of low energy as determined by Monte Carlo calculations. Therefore, the hirudin peptide must contain stabilizing interactions in favor of the conformation in the thrombin-bound state. These interactions may come primarily from hydrophobic contacts between the side chains of Phe(56), Ile(59), Pro(60), Tyr(63), and Leu(64). In the complex, the side chain of the hirudin residue, Ile(59), is located at the center of a cluster of nonpolar residues from both hirudin and the thrombin exosite (Figure 6). In solution, Ile(59) also seems to serve as a bridge between Phe(56) and the nonpolar face of the tight 3_{10}-helix, stabilizing the global amphiphilic structure of the peptide (Figure 5). This critical role of Ile(59) may account for the importance of this residue in determining the inhibitory activities of the hirudin peptide (Yue et al., 1991).

The existence of ordered conformations of the free hirudin peptide in solution calls for a more detailed characterization of the conformational ensemble accessible by the peptide. In terms of the peptide backbone, only partial helicities (~50%) were observed for residues Glu(61)–Leu(64) in both aqueous solution and the mixed solvent. These helical contents must contain a large fraction of the active 3_{10}-helical conformations as indicated by the extensive medium-range NOE's involving the last six residues of the peptide (Table II). The bound rotameric states for Phe(56), Tyr(63), and Leu(64) are the most populated ones in solution, while for Ile(59), the bound conformation is apparently the lower populated one (<40%). Furthermore, NOE's involving the side chain of Ile(59) indicate that the folded conformation of the free hirudin peptide may adopt a trans ($\chi_1 = -60$) conformation for the side chain of Ile(59) in contrast to the gauche$^-$ ($\chi_1 = +60$) state observed in the thrombin-bound state (Figure 6). However, conformational searches using molecular dynamics and Monte Carlo simulations revealed that the gauche$^-$ ($\chi_1 = +60$) side-chain conformation of Ile(59) is also a stable rotamer within the thrombin-bound conformation of the entire peptide (Figure 5). It is not clear as to why thrombin would prefer to bind to the peptide with a gauche$^-$ ($\chi_1 = +60$) side-chain conformation for Ile(59). In the thrombin exosite, there is a positively charged residue, Arg(67), among the hydrophobic residues that are in contact with the hirudin COOH-terminal peptide (Figure 6). This Arg residue of thrombin is situated in close proximity to the hydrophobic side chain of Ile(59) in the hirudin peptide (Rydel et al., 1990; Yue et al., 1991). The ethyl group of Ile(59) is directed, by the gauche$^-$ χ_1 conformation of Ile(59), toward a cavity within the hydrophobic cluster formed between the thrombin residues Leu(65), Tyr(76), Ile(82), and Met(84) and the hirudin residues Ile(59), Pro(60), Tyr(63), and Leu(64). There would be unfavorable interactions between the polar and charged side chain of the thrombin residue, Arg(67), and the nonpolar side chain (particularly the ethyl group) of the hirudin residue Ile(59), if the side chain of Ile(59) is to assume the trans conformation favored in the free peptide. NMR studies are in progress to characterize the importance of Ile(59) in the interaction of hirudin peptides to thrombin.

Conclusion. The folding of hirudin 55–65 has been assessed by an NMR analysis of the peptide fragment in solution and in the thrombin-bound state. In solution, the peptide assumes a highly populated conformation with structural features that are quite similar to those recognized by thrombin. Both molecular dynamics simulations and Monte Carlo conformational searches suggest that the thrombin-bound structure of the peptide is of low energy and intrinsically stable in solution. The stability of the active conformation seems to be a result of hydrophobic interactions between nonpolar residues that are essential for inhibitory activity.

ACKNOWLEDGMENTS

We thank Jean Lefebvre for peptide synthesis and purification and Bernard F. Gibbs for amino acid analysis. We also acknowledge Drs. J. DiMaio and Y. Konishi for helpful discussions.

SUPPLEMENTARY MATERIAL AVAILABLE

Tables SI and SII listing the proton resonance assignments for hirudin 55–65 in both aqueous and the mixed solvents at 25 and 0 °C and Table SIII containing the lists of ECEPP/2 energies and backbone dihedral angles for the stable conformations observed during molecular dynamics and EDMC simulations (4 pages). Ordering information is given on any current masthead page.

REFERENCES

Andersen, N. H., Nguyen, K. T., Hartzell, C. J., & Eaton, H. L. (1987) *J. Magn. Reson. 74*, 195.

Bax, A., & Davis, D. (1985) *J. Magn. Reson. 63*, 207.
Bax, A., Sklenar, V., & Summers, M. P. (1986) *J. Magn. Reson. 70*, 327.
Berliner, L. J., Sugawara, Y., & Fenton, J. W., II (1985) *Biochemistry 24*, 7005.
Bode, W., Mayr, I., Baumann, U., Huber, R., Stone, S. R., & Hofsteenge, J. (1989) *EMBO J. 8*, 3467.
Bothner-By, A. A., Stephens, R. L., Lee, J.-M., Warren, C. D., & Jeanloz, R. W. (1984) *J. Am. Chem. Soc. 106*, 811.
Bradley, E. K., Thomason, J. F., Cohen, F. E., Kosen, P. A., & Kuntz, I. D. (1990) *J. Mol. Biol. 215*, 607.
Braun, P. J., Dennis, S., Hofsteenge, J., & Stone, S. R. (1988) *Biochemistry 27*, 6517.
Bystrov, V. F. (1976) *Prog. Nucl. Magn. Reson. Spectrosc. 10*, 41.
Cantor, C. R., & Schimmel, P. R. (1980) *Biophysical Chemistry*, W. H. Freeman and Co., San Francisco, CA.
Chang, J. Y. (1989) *J. Biol. Chem. 264*, 7141.
Chang, J. Y. (1990) *J. Biol. Chem. 265*, 22159.
Chang, J. Y., Ngai, P. K., Rink, H., Dennis, S., & Schlaeppi, J. M. (1990a) *FEBS Lett. 261*, 287.
Chang, J. Y., Schlaeppi, J. M., & Stone, S. R. (1990b) *FEBS Lett. 260*, 209.
Clore, G. M., Sukumaran, D. K., Nilges, M., Zarbock, J., & Gronenborn, A. M. (1987) *EMBO J. 6*, 529.
Cowburn, D., Live, D. H., Fischman, A. J., & Agosta, W. C. (1983) *J. Am. Chem. Soc. 105*, 7435.
Dennis, S., Wallace, A., Hofsteenge, J., & Stone, S. R. (1990) *Eur. J. Biochem. 188*, 61.
Dietrich, W., Rüdel, C. H., & Neumann, M. (1991) *J. Magn. Reson. 91*, 1.
DiMaio, J., Gibbs, B., Munn, D., Lefebvre, J., Ni, F., & Konishi, Y. (1990) *J. Biol. Chem. 265*, 21698.
DiMaio, J., Ni, F., Gibbs, B., & Konishi, Y. (1991) *FEBS Lett. 282*, 47.
Dodt, J., Köhler, S., Schmitz, T., & Wilhelm, B. (1990) *J. Biol. Chem. 265*, 713.
Dyson, H. J., Rance, M., Houghten, R. A., Wright, P. E., & Lerner, R. A. (1988) *J. Mol. Biol. 201*, 201.
Eaton, H. L., & Andersen, N. H. (1987) *J. Magn. Reson. 74*, 212.
Farmer, B. T., II, Macura, S., & Brown, L. R. (1987) *J. Magn. Reson. 72*, 347.
Fenton, J. W., II (1981) *Ann. N.Y. Acad. Sci. 370*, 468.
Fenton, J. W., II, Olson, T. A., Zabinski, M. P., & Wilner, G. D. (1988) *Biochemistry 27*, 7106.
Fischman, A. J., Wyssbrod, H. R., Agosta, W. C., & Cowburn, D. (1978) *J. Am. Chem. Soc. 100*, 54.
Folkers, P. J. M., Clore, G. M., Driscoll, P. C., Dodt, J., Köhler, S., & Gronenborn, A. M. (1989) *Biochemistry 28*, 2601.
Gay, D. M. (1983) *Assoc. Comput. Mach. Trans. Math. Software 9*, 503.
Griesinger, C., & Ernst, R. R. (1987) *J. Magn. Reson. 75*, 261.
Grütter, M. G., Priestle, J. P., Rahuel, J., Grossenbacher, H., Bode, W., Hofsteenge, J., & Stone, S. R. (1990) *EMBO J. 9*, 2361.
Haruyama, H., & Wüthrich, K. (1989) *Biochemistry 28*, 4301.
Haruyama, H., Qian, Y. Q., & Wüthrich, K. (1989) *Biochemistry 28*, 4312.
Hayashi, T., Zushi, M., Yamamoto, S., & Suzuki, K. (1990) *J. Biol. Chem. 265*, 20156.
Hortin, G. L., Tollefsen, D. M., & Benutto, B. M. (1989) *J. Biol. Chem. 264*, 13979.
Jakubowski, J. A., & Maraganore, J. M. (1990) *Blood 75*, 399.
Jorgensen, W., Chandrasekhar, J., Madura, J., Impey, R., & Klein, M. (1983) *J. Chem. Phys. 79*, 926.
Kaminski, M., & McDonagh, J. (1983) *J. Biol. Chem. 258*, 10530.
Kaminski, M., & McDonagh, J. (1987) *Biochem. J. 242*, 881.
Kim, Y., & Prestegard, J. H. (1989) *J. Magn. Reson. 84*, 9.
Krstenansky, J. L., Owen, T. J., Yates, M. T., & Mao, S. J. T. (1987) *J. Med. Chem. 30*, 1688.
Krstenansky, J. L., Owen, T. J., Yates, M. T., & Mao, S. J. T. (1988) *Biochim. Biophys. Acta 957*, 53.
Krstenansky, J. L., Broersma, R. J., Owen, T. J., Payne, M. H., Yates, M. T., & Mao, S. J. (1990) *Thromb. Haemostasis 63*, 208.
Mao, S. J. T., Yates, M. T., Owen, T. J., & Krstenansky, J. L. (1988) *Biochemistry 27*, 8170.
Maraganore, J. M., Chao, B., Joseph, M. L., Jablonski, J., & Ramachandran, K. L. (1989) *J. Biol. Chem. 264*, 8692.
Maraganore, J. M., Bourdon, P., Jablonski, J., Ramachandran, K. L., & Fenton, J. W., II (1990) *Biochemistry 29*, 7095.
Marion, D., & Bax, A. (1989) *J. Magn. Reson. 83*, 205.
Marion, D., Ikura, M., & Bax, A. (1989) *J. Magn. Reson. 84*, 425.
Markwardt, F. (1970) *Methods Enzymol. 19*, 924.
Momany, F. A., McGuire, R. F., Burgess, A. W., & Scheraga, H. A. (1975) *J. Phys. Chem. 79*, 2361.
Naski, M. C., Fenton, J. W., II, Maraganore, J. M., Olson, S. T., & Shafer, J. A. (1990) *J. Biol. Chem. 265*, 13484.
Némethy, G., Pottle, M. S., & Scheraga, H. A. (1983) *J. Phys. Chem. 87*, 1883.
Neuhaus, D., & Keeler, J. (1986) *J. Magn. Reson. 68*, 568.
Neuhaus, D., & Williamson, M. P. (1989) *The Nuclear Overhauser Effect*, VCH Publishers, New York.
Ni, F., & Scheraga, H. A. (1986) *J. Magn. Reson. 70*, 506.
Ni, F., & Scheraga, H. A. (1989) *J. Magn. Reson. 82*, 413.
Ni, F., Konishi, Y., Frazier, R. B., Scheraga, H. A., & Lord, S. T. (1989a) *Biochemistry 28*, 3082.
Ni, F., Konishi, Y., Bullock, L. D., Rivetna, M. N., & Scheraga, H. A. (1989b) *Biochemistry 28*, 3106.
Ni, F., Meinwald, Y. C., Vásquez, M., & Scheraga, H. A. (1989c) *Biochemistry 28*, 3094.
Ni, F., Konishi, Y., & Scheraga, H. A. (1990) *Biochemistry 29*, 4479.
Otting, G., Widmer, H., Wagner, G., & Wüthrich, K. (1986) *J. Magn. Reson. 66*, 187.
Pachler, K. G. R. (1963) *Spectrochim. Acta 19*, 2085.
Prescott, S. M., Seeger, A. R., Zimmerman, G. A., McIntyre, T. M., & Maraganore, J. M. (1990) *J. Biol. Chem. 265*, 9614.
Ragg, H., Ulshofer, T., & Gerewitz, J. (1990) *J. Biol. Chem. 265*, 5211.
Ripoll, D. R., & Scheraga, H. A. (1988) *Biopolymers 27*, 1283.
Ripoll, D. R., & Scheraga, H. A. (1989) *J. Protein Chem. 8*, 263.
Ripoll, D. R., & Ni, F. (1992) *Biopolymers* (in press).
Ryckaert, J. P., Ciccotti, G., & Berendsen, H. J. C. (1977) *J. Comput. Phys. 23*, 327.
Rydel, T. J., Ravichandran, K. G., Tulinsky, A., Bode, W., Huber, R., Roitsch, C., & Fenton, J. W., II (1990) *Science 249*, 277.

Scheraga, H. A. (1986) *Ann. N.Y. Acad. Sci. 485*, 124.
Sippl, M. J., Némethy, G., & Scheraga, H. A. (1984) *J. Phys. Chem. 79*, 2361.
Stanfield, R. L., Fieser, T. M., Lerner, R. A., & Wilson, I. A. (1990) *Science 248*, 712.
Stimson, E. R., Meinwald, Y. C., Montelione, G. T., & Scheraga, H. A. (1986) *Int. J. Pept. Protein Res. 27*, 569.
Stone, S. R., & Hofsteenge, J. (1986) *Biochemistry 25*, 4622.
Stone, S. R., Dennis, S., & Hofsteenge, J. (1989) *Biochemistry 28*, 6857.
Sukumaran, D. K., Clore, G. M., Preuss, A., Zarbock, J., & Gronenborn, A. M. (1987) *Biochemistry 26*, 333.
Tsiang, M., Lentz, S. R., Dittman, W. A., Wen, D., Scarpati, E. M., & Sadler, J. E. (1990) *Biochemistry 29*, 10602.
Verlet, L. (1967) *Phys. Rev. 159*, 98.
Vu, T.-K. H., Hung, D. T., Wheaton, V. I., & Coughlin, S. R. (1991) *Cell 64*, 1057.
Wagner, G., Neuhaus, D., Wörgötter, E., Vasak, M., Kagi, J. H. R., & Wüthrich, K. (1984) *J. Mol. Biol. 187*, 131.
Weiner, S. J., Kollman, P. A., Case, D. C., Singh, U. C., Ghio, C., Alagona, G., Profeta, S., Jr., & Weiner, P. (1984) *J. Am. Chem. Soc. 106*, 765.
Wright, P. E., Dyson, H. J., & Lerner, R. A. (1988) *Biochemistry 27*, 7167.
Yue, S.-Y., DiMaio, J., Szewczuk, Z., Purisima, E. O., Ni, F., & Konishi, Y. (1991) *Protein Eng.* (in press).

The Ca^{2+} Ion and Membrane Binding Structure of the Gla Domain of Ca-Prothrombin Fragment 1[†,‡]

M. Soriano-Garcia,[§,∥] Kaillathe Padmanabhan,[§] A. M. de Vos,[⊥] and A. Tulinsky*[,§]

Department of Chemistry, Michigan State University, East Lansing, Michigan 48824, and Department of Protein Engineering, Genentech, Incorporated, 460 San Bruno Boulevard, South San Francisco, California 94080

Received September 17, 1991; Revised Manuscript Received December 11, 1991

ABSTRACT: The structure of Ca-prothrombin fragment 1 (residues 1–156 prothrombin) has been solved and refined at 2.2-Å resolution by X-ray crystallographic methods. The first two-thirds of the Gla domain (residues 1–48) and two carbohydrate chains (~5 kDa) are disordered in crystals of apo-fragment 1. When crystals are grown in the presence of Ca^{2+} ions, the Gla domain exhibits a well-defined structure binding seven Ca^{2+} ions, but the carbohydrate is still disordered. Even so, the crystallographic *R* factor reduced to 0.171. The folding of the Gla domain is dominated by 9–10 turns of three different α-helices. These turns produce two internal carboxylate surfaces composed of Gla side chains. A polymeric array of five Ca^{2+} ions separated by about 4.0 Å intercalates between the carboxylate surfaces. The coordination of the Ca^{2+} ions with Gla carboxylate oxygen atoms and water molecules leads to distorted polyhedral arrangements with μ-oxo bridges in a highly complex array that most likely orchestrates the folding of the domain. The overall mode of interaction of the Ca^{2+} ions is new and different from any Ca^{2+} ion–protein interactions heretofore observed or described. The fluorescence quenching event observed upon Ca^{2+} ion binding is due to a disulfide–π-electron interaction that causes a 100° reorientation of Trp42 of the Gla domain. The Ca^{2+} ion interaction also affords the N-terminus protection from acetylation because the latter is buried in the folded structure and makes hydrogen-bonding salt bridges with Gla17, Gla21, and Gla27. The Gla domain and its trailing disulfide unit associate intimately and together give rise to a domain-like structure. Electrostatic potential calculations indicate that the Gla domain is very electronegative. Since most of the carboxylate oxygen atoms of Gla residues are involved in Ca^{2+} ion binding, leaving only a few for bridging Ca^{2+} ion–phospholipid interactions, the role of bridging Ca^{2+} ions might be generally unspecific, with Ca^{2+} ions simply intervening between the negative Gla domain and negative head groups of the membrane surface. The folding of the kringle structure in apo- and Ca-fragment 1 is essentially the same. However, the Ser36–Ala47 helix of the Gla domain pivots around Cys48, shifting by approximately 30°, and the helix encroaches on the kringle producing some concomitant changes. These might be related to the protection of carbohydrate carrying Asn101 from acetylation in the Ca-fragment 1 structure.

Prothrombin is one of several proenzymes of blood involved in coagulation that undergoes posttranslational modification of glutamic acid residues in the N-terminal 48 or so residues to Gla[1] via a vitamin K dependent carboxylase (others are factors VII, IX, and X and the proteins designated C, S, and Z). The Gla residues vary in total number from 9 to 12 (Tulinsky et al., 1988) of which the first 10 are highly conserved (Figure 1). The function of the N-terminal residues of these zymogens is binding to membrane in the presence of Ca^{2+} ion (Gitel et al., 1973; Nelsestuen et al., 1974; Stenflo et al., 1974; Bajaj et al., 1975). They also bind Mg^{2+}, Sr^{2+}, and other metal ions (Furie et al., 1976; Bajaj et al., 1976; Nelsestuen et al., 1976; Bloom & Mann, 1978). Except for Sr^{2+} ions, the conformational change accompanying binding

[†] This work was supported by NIH Grant HL 25942.
[‡] The coordinates of the Ca-fragment 1 structure have been deposited in the Brookhaven Protein Data Bank (access no. 1PF2).
* To whom correspondence should be addressed.
[§] Michigan State University.
[∥] Present address: Instituto de Quimica, UNAM, Delegacion Coyoacan, Mexico D.F. 04510.
[⊥] Genentech, Inc.

[1] Abbreviations: Gla, γ-carboxyglutamic acid; fragment 1, prothrombin residues 1–156; ISIR, iterative single isomorphous replacement; EGF, epidermal growth factor; ANS, 1-anilinonaphthalene-8-sulfonate; fragment 1·2, prothrombin residues 1–274.

0006-2960/92/0431-2554$03.00/0